Universal Scaling and Fano Resonance in the Plasmon Coupling between Gold Nanorods

Kat Choi Woo,[†,§] Lei Shao,[†,§] Huanjun Chen,[†] Yao Liang,[†] Jianfang Wang,[†,*] and Hai-Qing Lin[†,‡,*]

[†]Department of Physics, The Chinese University of Hong Kong, Shatin, Hong Kong SAR and [‡]Beijing Computational Science Research Center, Beijing 100084, China. [§]These authors contributed equally to this work.

Noble metal nanostructures can support localized surface plasmon resonances when interacting with electromagnetic radiations. When they are placed close to each other, their plasmons are coupled together, leading to plasmon resonance shifts and the strong squeezing of light in the gap regions. These unique features brought about by the plasmon coupling between metal nanocrystals have been subjected to intensive research owing to their great potential in various applications. For example, distance-dependent, plasmon-coupling-induced spectral changes can serve as molecular rulers.[1] They have been taken as the basis for the development of highly sensitive biological and chemical sensors,[2] optical switches,[3] and metallic nanoscale lenses.[4] The local electric field enhancements arising from the adjacent placement of two metal nanocrystals is much larger than those associated with spatially isolated ones. The enormous field enhancements obtained from the plasmon coupling have already been utilized in various types of plasmon-enhanced spectroscopies (Raman, upconversion, one- and two-photon-excited fluorescence),[5−8] high-harmonic signal amplification,[9] and nanometric optical tweezers.[10]

A great number of investigations have been made to understand[11−24] and engineer[25−27] the plasmon coupling between metal nanocrystals. A majority of the previous studies have focused on the role of the spatial arrangement of metal nanocrystals, especially the gap distance, in the plasmon coupling. Specifically, for the homodimers of metal nanocrystals, such as elliptical and circular Au nanodisks,[11,15] Ag nanodisks,[14] and Au nanorods,[19,21] the fractional plasmon wavelength shifts have been found by either experimental or computational means to decay nearly exponentially with

ABSTRACT The plasmon coupling between metal nanocrystals can lead to large plasmon shifts, enormous electric field enhancements, and new plasmon modes. Metal nanorods, unlike spherical ones, possess a transverse and a longitudinal plasmon mode owing to their geometrical anisotropy. Consequently, the plasmon coupling between metal nanorods is much more complicated than that between nanospheres. For the latter, experimental approaches, simple scaling relationships, and exact analytic solutions have been developed for describing the plasmon coupling. In this study, we have carried out extensive finite-difference time-domain simulations to understand the plasmon coupling in the dimers of Au nanorods that are aligned along their length axes. The effects of the gap distance, longitudinal plasmon energy, and end shape of the nanorod monomers on the plasmon coupling have been scrutinized. The coupling energy diagrams show a general anticrossing behavior. All of them can be rescaled into one simple and universal hyperbolic formula. A theoretical model based on two interacting mechanical oscillators has been developed to understand the plasmon coupling between two arbitrarily varying Au nanorods. This model, together with the universal equation, allows for the determination of the coupled plasmon energies of Au nanorod dimers with high accuracies. Furthermore, the Fano interference has been observed in the nanorod heterodimers, with its behavior being dependent on the gap distance and plasmon energies of the nanorod monomers. Our results will be useful for predicting the coupled plasmon energies of metal nanorod dimers in a variety of plasmonic applications and understanding the Fano resonance in plasmonic nanostructures.

the interparticle gap distance. The ratios between the decay lengths and the characteristic sizes of the nanocrystal monomers are typically in the range 0.2−0.3, irrespective of the nanocrystal size, shape, or metal type or the refractive index of the surrounding medium.

Heterodimers of metal nanocrystals exhibit more complex plasmon coupling behaviors than homodimers because the symmetry breaking in the heterodimers leads to the formation of new plasmon modes. The interaction between different plasmon modes, usually broad superradiant "bright" modes and narrow subradiant "dark" modes, can give rise to the Fano resonance in asymmetric plasmonic nanostructures.[28,29] When

the Fano resonance occurs, the asymmetrical Fano profile with a clear Fano minimum that results from a destructive interference appears in the spectral responses. This plasmonic Fano interference phenomenon can not only further our understanding on light–matter interactions at the nanoscale below the diffraction limit of light but also offer tremendous potential for developing various plasmonic devices. The Fano resonance has so far been observed in several types of metal nanocrystal heterodimers.[30−32] The symmetry breaking in the heterodimers plays an important role in the generation of the Fano interference. The unique properties of the Fano resonance have been utilized for creating nanoscale sensors with improved performance,[33] fabricating metamaterials with very narrow and nearly full transparency windows,[34] and realizing various active operations, such as optical switching[32] and electro-optical modulation.[35]

Gold nanorods are one type of preferred candidates for future plasmonic applications owing to their synthetically tunable longitudinal plasmon energies, polarization-sensitive longitudinal plasmon modes, and simple and reliable synthetic protocols. Controllable plasmonic coupling between Au nanorods can provide adjustable resonance frequencies as well as superior local field enhancements. It is therefore strongly desirable for the development of high-efficiency optical antennas,[36,37] ultrasensitive biosensors, and high-performance plasmon-enhanced quantum emitters. Tailoring the plasmon coupling in Au nanorod dimers can be realized either by varying the interparticle gap distance or by adjusting the plasmon energies of the nanorods. The latter can result in controllable coupled plasmon energies while the gap distance remains unchanged. This controllability will be advantageous to applications that require simultaneously large local field enhancements and variable plasmon energies. Consequently, there exists a strong need to evaluate the coupled plasmon energies in the design of plasmonic structures and devices out of plasmon-coupled Au nanorods. A plasmon-hybridization model has been developed for the determination of the coupled plasmon energies of both homo- and heterodimers of metal nanorods in the quasi-static limit.[18,38] The effect of the symmetry breaking on the plasmon coupling in Au nanorod dimers has been examined in a recent study.[39] At a maintained gap distance, the coupled plasmon energy has been found to be strongly dependent on the plasmon energy of each nanorod monomer. In our previous work, the coupled plasmon energies of the dimers composed of mismatched Au nanorods have also been measured, and an anticrossing behavior has been observed in the plasmon coupling energy diagram.[22] Despite these previous efforts and in contrast to the occurrence of a number of studies on the distance dependence of the plasmon coupling, simple and reliable means have not been found for the determination of the coupled plasmon energies of Au nanorod dimers. The coupled plasmon energies of Au nanorod dimers are strongly dependent on both the plasmon energies of and the gap distance between the nanorod monomers. The interplay of these two dependences makes the accurate prediction of the coupled plasmon energies rather challenging.

Here we report on our systematic study of the energy diagrams of the plasmon coupling between Au nanorods that are aligned along their length axes using the finite-difference time-domain (FDTD) simulation method. The coupled plasmon energy has been investigated as a function of the plasmon energy of the nanorod monomer, the nanorod end shape, and the gap distance between the nanorod monomers. All of the coupling energy diagrams can be collapsed onto one universal scaling curve. A theoretical model based on two interacting mechanical oscillators has also been employed to understand the plasmon coupling in Au nanorod dimers. Moreover, the asymmetric nanorod heterodimers are found to exhibit the Fano resonance. The parameters obtained from fitting the scattering spectra with the Fano profile are dependent on the relative plasmon energies of the nanorod monomers and the interparticle gap distance.

RESULTS AND DISCUSSION

A commercial package, FDTD Solutions 6.5, which was developed by Lumerical Solutions, was employed for the simulations. Au nanorods were modeled as cylinders with differently shaped end-caps. Each nanorod had a radius R of 10 nm. The total length of the nanorod L was varied from 20 to 100 nm. The aspect ratio $L/(2R)$ was therefore varied from 1 to 5. Such sizes are typical for chemically synthesized colloidal Au nanorods.[40−42] The nanorods were placed in a linear end-to-end configuration to form dimers, because colloidal Au nanorods tend to assemble in a linear end-to-end manner in liquids.[25,43−48] The gap distance between the two nanorods was also variable. The dielectric function of gold was described by the Drude model with parameters chosen to match the experimental dielectric data as close as possible. The refractive index of the surrounding medium was set to be 1.33, which is the refractive index of water. For our simulations, 0.5 nm spatial discretization was used in the gap region and 1 nm grids were applied in other regions. The excitation light was polarized along the length axis of the nanorod, which is also the axis of rotational symmetry of the dimer system. The transverse polarized light was not taken into account, since the plasmon resonance excited by such polarization is very weak in comparison to the longitudinal plasmon resonance for typically sized Au nanorods.[22,39]

Figure 1a shows the calculated scattering spectra of two Au nanorod monomers as examples. The nanorods
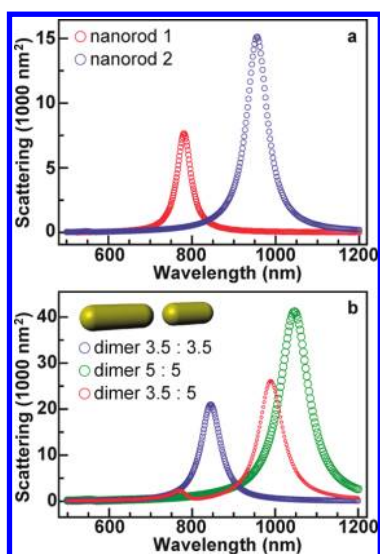
Figure 1. (a) Scattering spectra of two differently sized Au nanorods with hemispherical ends. The aspect ratios of the nanorods 1 and 2 are 3.5 and 5, respectively. (b) Scattering spectra of the plasmon-coupled Au nanorod dimers. The gaps between the two nanorods in all three dimers are 7 nm. The inset shows schematically the heterodimer.

are capped with hemispheres at their ends. The aspect ratios of the two nanorods are 3.5 and 5, respectively. Their scattering spectra exhibit sharp peaks at 781 and 956 nm, respectively, which are ascribed to the long-itudinal plasmon resonance wavelengths of the nano-rods. The calculated longitudinal plasmon wavelengths exhibit a linear dependence on the aspect ratios of the nanorods (Supporting Information, Figure S1). This linear dependence is in agreement with previous experimental findings.[19,22,42] We can then vary the longitudinal plasmon energy of the Au nanorod by changing the aspect ratio. In addition, because max-imum scattering occurs when the localized plasmon resonances of metal nanocrystals are resonantly ex-cited, the plasmon energies were obtained from the peak wavelengths of the calculated scattering spectra of the Au nanorod monomers and dimers in our study.

Figure 1b shows the calculated scattering spectra of the plasmon-coupled Au nanorod dimers. There are two homodimers and one heterodimer (Figure 1b, inset). The gap distances in all of the dimers are set at $d = 7$ nm. When the homodimers are formed from the nanorods with aspect ratios of 3.5 and 5, the plasmon resonance peaks red-shift to 845 and 1047 nm, respectively, due to the capacitive attraction between the two nanorods. The plasmon coupling between two identical nanorods can be well understood on the basis of the hybridization model.[18,38] The red-shifted hybri-dized plasmon mode in the nanorod homodimers is known as a hybridized bonding mode. Owning to the symmetry of the structure, the corresponding anti-bonding one cannot be excited by far-field light. It is known as a "dark" mode. When the two different nanorods are placed together to form the heterodimer,

a weak scattering peak in the shorter-wavelength region, in addition to the strong scattering peak in the longer-wavelength region, is produced. The two scattering peaks are positioned at 770 and 989 nm, respectively. The higher-energy peak is induced by the symmetry breaking in the heterodimer. A detailed discussion about it will be presented later in this study. We first examined how the coupled plasmon energy of the bonding mode is dependent on the nanorod monomers. In our previous experimental study,[22] we have observed an anticrossing behavior in the plas-mon coupling energy diagram of Au nanorod dimers. Due to the experimental limitations, only one coupling energy diagram at a particular gap distance has been obtained. FDTD simulations allow the parameters in-volved in the plasmon coupling to be varied over a large parameter space. We therefore carried out sys-tematic FDTD simulations in order to gain a deeper understanding of the plasmon coupling behavior in Au nanorod dimers.

In our simulations, we fixed the plasmon energy of one nanorod and varied that of the other. For Au nanorods with hemispherical ends, the plasmon en-ergy of a nanorod monomer varies from 2.466 to 1.297 eV when the aspect ratio is changed from 1 to 5 (Supporting Information, Table S1). An aspect ratio of 1 for a nanorod with hemispherical ends corresponds to a nanosphere. A plasmon coupling energy diagram for a representative nanorod dimer is given in Figure 2a. For this example, the plasmon energy, E_{fixed}, of one nanorod is fixed at 1.715 eV (red circles). The gap distance is set at $d = 1$ nm. As the plasmon energy of the other nanorod is gradually increased (black circles), the coupled plasmon energy of the dimer also in-creases (blue circles). It is always smaller than the plasmon energies of the two nanorod monomers. The increase saturates asymptotically toward the plas-mon energy of the fixed nanorod. The coupling energy diagram therefore exhibits an anticrossing behavior. This anticrossing behavior is maintained when E_{fixed} is varied from 1.297 to 2.466 eV, as shown in Figure 2b. The saturation limit of the coupled plasmon energy gets larger with increasing E_{fixed}. The numerical values of the coupled plasmon energies for all of the dimers are supplied in Table S2 in the Supporting Information.

One of our aims in this study is to find out whether and how the plasmon coupling between variously sized Au nanorods can be unified with a simple scaling relationship. Interestingly, we found that all of the anticrossing energy diagrams collapse into one if both the plasmon energies of the nanorod monomers and the coupled plasmon energies are divided by their corresponding E_{fixed} (Figure 2c). The universal rescaled energy diagram might result from the fact that the plasmon coupling strength is mainly determined by the gap distance. Once a gap distance is given, the strength of the electromagnetic interaction between
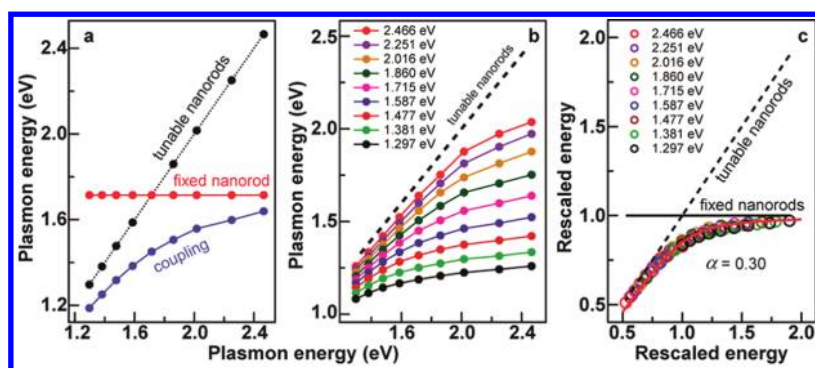
Figure 2. Energy diagrams of the plasmon coupling between Au nanorods with hemispherical ends at a fixed gap distance of 1 nm. (a) Plasmon coupling between one nanorod with a fixed aspect ratio and another nanorod with varying aspect ratios. The blue, black, and red circles represent the coupled plasmon energy, plasmon energy of the varying nanorod, and plasmon energy of the fixed nanorod, respectively. The three energies are plotted as functions of the plasmon energy of the varying nanorod. (b) Coupled plasmon energy curves obtained when the aspect ratio of the fixed nanorod is set at different values. The corresponding plasmon energies of the fixed nanorods are given in the inset. The horizontal lines for the fixed nanorods are omitted for clarity. (c) Rescaled energy diagram of the plasmon coupling between variously sized nanorods from (b). The coefficient of determination for the fitting is $R^2 = 0.9996$.

the nanorods will be fixed. Figure 2c shows that the universal diagram has two asymptotes. One is the inclined line with a slope of 1 (dashed line), and the other is the horizontal line (black line). We therefore utilized a hyperbolic function to describe the rescaled coupled plasmon energies

$$y = 0.5(x+1) - 0.5\sqrt{(x-1)^2 + \alpha^2} \quad (1)$$

In eq 1, x and y are the rescaled energy values on the horizontal and vertical axis, respectively. There is only one fitting parameter, α, in the equation. When $\alpha = 0.30$, the hyperbolic equation fits very well the universal energy diagram, with a coefficient of determination of $R^2 = 0.9996$.

We next considered the effect of the interparticle gap distance on the plasmon coupling between Au nanorods. We performed the FDTD calculations of the Au nanorod dimers with the two monomers having varying plasmon energies and spaced apart at $d = 3, 5,$ and 7 nm, respectively. The calculated coupled plasmon energy values are listed in Tables S3, S4, and S5 of the Supporting Information. At each gap distance, all of the coupling energy diagrams are collapsed onto one (Figure 3a–c). In addition, we also calculated the coupled plasmon energies of the nanorod dimers with a gap distance of 7 nm immersed in media having varying refractive indices. The results (Supporting Information, Figure S2 and Table S6) show that the plasmon coupling energy diagrams obtained for different refractive indices also collapse universally onto one curve. Therefore, the effect of the index of the surrounding medium can also be included in the energy rescaling. In this study, we focus on the plasmon coupling behavior of the nanorod dimers in water. The rescaled anticrossing energy diagrams can be well fitted with the hyperbolic function given above. The parameter α/coefficient of determination R^2 obtained from the fitting are 0.20/0.9998, 0.16/0.9998,

and 0.14/0.9999 for $d = 3, 5,$ and 7 nm, respectively. α is seen to decrease as d is increased. A close examination of Figure 2c and Figure 3a–c indicates that the coupling-induced plasmon shift also decreases with increasing gap distances. The decreased plasmon shift is attributed to the reduced capacitive coupling between the nanorods. We therefore reason that the fitting parameter α is dependent on the plasmon coupling strength.

The fractional plasmon shift is directly related to the plasmon coupling strength. In order to ascertain how α changes with the fractional plasmon shift, we carried out the FDTD simulations on Au nanorod dimers with the gap distance between the two nanorods varied from 2 to 24 nm at a step of 2 nm. For each gap distance, since the results above have shown that all of the coupling energy diagrams can be rescaled onto a universal curve, we fixed the plasmon energy of one nanorod at $E_{fixed} = 2.016$ eV and changed the plasmon energy of the other nanorod. All of the as-calculated coupled plasmon energies are listed in Table S7 in the Supporting Information. They were thereafter subjected to the rescaling and hyperbolic fitting so that α could be determined. We then plotted α as a function of $\Delta E/E_{fixed}$ (Figure 3d), where ΔE is the difference between E_{fixed} and the coupled plasmon energy of the corresponding homodimer $E_{homodimer}$. For the data points shown in Figures 2c and 3a–c, there are many different E_{fixed} values. If all of the energy diagrams at each gap distance follow exactly the universal hyperbolic equation, then $E_{homodimer}/E_{fixed}$ and therefore $\Delta E/E_{fixed} = 1 - E_{homodimer}/E_{fixed}$ are fixed for different E_{fixed} values. α is seen to be proportional to $\Delta E/E_{fixed}$. A linear fitting gave a proportionality constant of $k = 2.06$ and a coefficient of determination of $R^2 = 0.9963$. The proportional relationship between α and $\Delta E/E_{fixed}$ supports our above argument that α can be interpreted as a
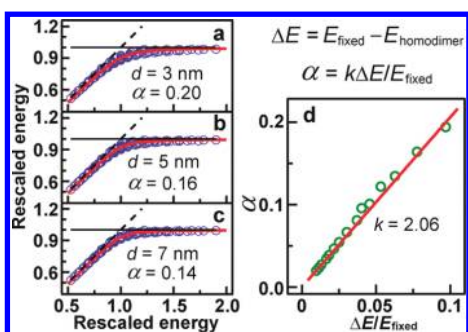
Figure 3. (a–c) Rescaled energy diagrams of the plasmon coupling between nanorods with hemispherical ends at different gap distances. The coefficients of determination for the fittings are 0.9998, 0.9998, and 0.9999, respectively. (d) Fitting parameter α as a function of the fractional plasmon energy shift $\Delta E/E_{fixed}$. The coefficient of determination for the linear fitting is $R^2 = 0.9963$.

measure of the plasmon coupling strength of Au nanorod dimers.

We also studied how the end shape of Au nanorods affects the plasmon coupling between Au nanorods. Previous studies have shown that the end curvature affects the longitudinal plasmon energy of Au nanorods.[22] Au nanorods with flat (Figure 4a, inset) and sharp ends (Figure 4b, inset) were considered. The sharp end was modeled with a hemiprolate spheroid, with the length of the major axis being twice that of the minor axis. The major axis is aligned along the length axis of the nanorod. For both types of nanorods, the gap distances were set to be 1, 3, 5, and 7 nm, and the aspect ratio of one nanorod monomer was kept at 3 to reduce the computational load. The plasmon energies of the nanorod monomers and dimers are provided in Tables S8 and S9 in the Supporting Information for the flat and sharp ends, respectively. Figure 4a and b show the rescaled energy diagrams when the gap distance is 1 nm. The energy diagrams can also be well fitted with eq 1. The obtained values for α are 0.46 and 0.27 for the flat and sharp ends, respectively. Taken together with the α value of 0.30 for the nanorods with hemispherical ends at $d = 1$ nm (Figure 2c), the results indicate that blunter ends lead to larger plasmon shifts for a given interparticle gap distance. This is understandable because the capacitive coupling between Au nanorods with blunter ends is stronger. Similar to the case of the nanorods with hemispherical ends, α also varies in proportion to $\Delta E/E_{fixed}$ for both types of end shapes as the gap distance is changed (Figure 4c,d). The proportionality constants obtained from linear fitting are both 1.95. These results reveal that the hyperbolic function described by eq 1 is suitable for predicting the coupled plasmon energies of the dimers of Au nanorods with different end shapes. The fitting parameter α is directly proportional to $\Delta E/E_{fixed}$. The proportionality constant is approximately equal to 2, irrespective of the end shape of Au nanorods.

Equation 1 is purely mathematical. We tried to translate the rescaled energies back into the physical
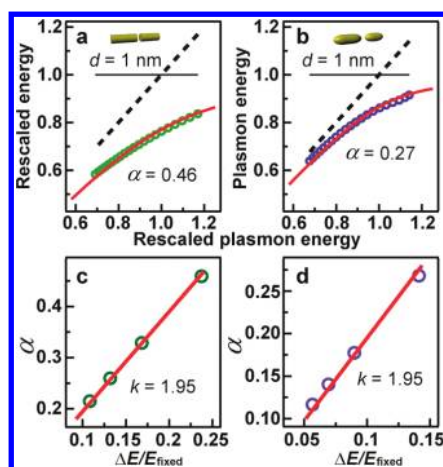

Figure 4. (a, b) Rescaled energy diagrams of the plasmon coupling between nanorods with flat and sharp ends, respectively. The insets show schematically the two types of dimers. The gap distances are both 1 nm. The coefficients of determination for the two fittings are 0.9999 and 0.9989. (c, d) Fitting parameter α as a function of $\Delta E/E_{fixed}$ for the flat and sharp nanorod dimers, respectively. The coefficients of determination for the fittings are 0.9999 and 0.9988, respectively.

parameters involved in the plasmon coupling in the Au nanorod dimers in order to gain the underlying physics. If E_1 and E_2 are used to represent the plasmon energies of the fixed and varying nanorod monomers, respectively, the coupled plasmon energy E_{12} can be obtained from eq 1 as

$$E_{12} = \frac{1}{2}(E_1 + E_2) - \frac{1}{2}\sqrt{(E_1 - E_2)^2 + [2(E_1 - E_{11})]^2}$$

(2)

where E_{11} is the coupled plasmon energy of the homodimer composed of the fixed nanorods. The term $E_1 - E_{11}$ in eq 2 represents the contribution from the plasmon coupling. Due to the exchangeability between the two nanorod monomers in a dimer, the second term under the square root in eq 2 can be replaced with $[2(E_2 - E_{22})]^2$. However, the plasmon coupling strength is also affected by the size and shape of the nanorod, although it is predominantly determined by the gap distance, as revealed by our FDTD simulations. The rescaled energy diagrams are seen to deviate slightly from the hyperbolic curve. As a result, the coupled plasmon energy E_{12} values calculated from $E_1 - E_{11}$ and $E_2 - E_{22}$ are not exactly the same. To reduce the error, we replace the term $E_1 - E_{11}$ with the average of $E_1 - E_{11}$ and $E_2 - E_{22}$, which gives

$$E_{12} = \frac{1}{2}(E_1 + E_2) - \frac{1}{2}\sqrt{(E_1 - E_2)^2 + [(E_1 - E_{11}) + (E_2 - E_{22})]^2}$$

(3)

The largest error in the coupled plasmon energies calculated with eq 3 in comparison with the FDTD simulation results is 3.8%. Equation 3 therefore provides an analytical expression for the evaluation of the coupled plasmon energy between any two Au

nanorods that are placed adjacently in a linear end-to-end manner, once the plasmon energies of the corresponding nanorod monomers and homodimers that have the same gap distance are obtained in the same dielectric environment. The quick and reliable estimation of the coupled plasmon energies between Au nanorods will facilitate the plasmonic applications of Au nanorods in biotechnology and optics.

We further employed a theoretical model based on two coupled mechanical oscillators to help in understanding the plasmon coupling in Au nanorod dimers. We note that similar models have previously been used to understand electromagnetically induced transparency[49] and the Fano resonance in Au nanoparticle–silica layer–Au layer core–shell–shell nanostructures.[50] In our study, the coupled plasmon modes of Au nanorod dimers can be modeled as two mechanical oscillators with frequencies ω_1 and ω_2. The two oscillators interact through one spring with a coupling constant of α_0. In the absence of dissipation, the coupled-oscillator system can be described by the Lagrangian

$$L = T - V$$

$$= \frac{1}{2}\dot{x}_1^2 + \frac{1}{2}\dot{x}_2^2 - \frac{1}{2}\omega_1^2 x_1^2 - \frac{1}{2}\omega_2^2 x_2^2 + \alpha_0 x_1 x_2 \quad (4)$$

where T and V denote the kinetic and potential energies, x_1 and x_2 are the displacements from the equilibrium positions of the oscillators in a one-dimensional system, and the dots represent the time derivatives of the displacements. The Lagrangian equations of motion are given as

$$\frac{d}{dt}\left(\frac{\partial L}{\partial \dot{x}_i}\right) - \frac{\partial L}{\partial x_i} = 0 \quad (5)$$

The solutions to eq 5 are in the form of a linear combination of harmonics. A determinant equation can be generated by inserting the solutions into eq 5. Two solutions for the eigenoscillation frequency Ω are obtained by solving the determinant equation. Because the lower-energy coupled plasmon mode was considered in our above discussion of the coupled plasmon energies, the smaller eigenfrequency solution is taken. It is given by

$$\Omega^2 = \frac{(\omega_1 + \omega_2)^2}{4}\left\{\left[1 - \sqrt{\left(\frac{\omega_1 - \omega_2}{\omega_1 + \omega_2}\right)^2 + \frac{4\alpha_0^2}{(\omega_1 + \omega_2)^4}}\right]^2 - \frac{4\alpha_0^2}{(\omega_1 + \omega_2)^4}\right\} \quad (6)$$

By using Taylor expansion, the eigenfrequency of the coupled-oscillator system Ω can be expressed as

$$\Omega = \frac{\omega_1 + \omega_2}{2} - \frac{1}{2}\sqrt{(\omega_1 - \omega_2)^2 + \frac{4\alpha_0^2}{(\omega_1 + \omega_2)^2}} - \delta \quad (7)$$

The first two terms in eq 7 have nearly the same form as eq 3, which was obtained through the hyperbolic fitting.

The second term under the square root in eq 7 involves the coupling constant, α_0, of the spring connecting the two oscillators. It represents the perturbation of the coupling to the total energy of the coupled-oscillator system. In the nanorod dimer system, the term bringing the plasmon coupling into the total energy is represented by $[(E_1 - E_{11}) + (E_2 - E_{22})]^2$. The coupling strength between the two nanorods is therefore related to the difference in the plasmon energies of the nanorod monomers and the corresponding homodimers. If we let the corresponding terms in eqs 3 and 7 be equivalent to each other, δ/Ω in eq 7 is estimated to the first-order from our FDTD simulation data to be smaller than 3.5%. As a result, the δ term in the coupled plasmon energy of the Au nanorod dimer is neglected. The above reasoning indicates the usefulness of the coupled-oscillator model in understanding the coupled plasmon energy between Au nanorods.

Equation 3 can be employed to calculate the coupled plasmon energies between variously sized Au nanorods if the plasmon energies of the nanorod monomers and the corresponding homodimers having the same gap distance are known. The longitudinal plasmon energies of Au nanorod monomers can be determined either spectroscopically or from the linear dependence of the longitudinal plasmon wavelength on the nanorod aspect ratio.[19,22,42] We then need to find out the coupled plasmon energies of two identical Au nanorods that are aligned linearly. Previous studies[11,14,15] have shown that the coupled plasmon wavelength between two identical metal nanoparticles can be described using an empirical universal scaling law

$$\frac{\Delta\lambda}{\lambda} = \beta e^{-\left(\frac{d/D}{\tau}\right)} \quad (8)$$

where λ is the plasmon wavelength of the individual metal nanoparticle, $\Delta\lambda$ is the plasmon wavelength shift arising from the plasmon coupling, d is the gap distance, D is the diameter of the nanoparticle, τ is the decay constant, and β is the maximum fractional plasmon wavelength shift. The decay constant τ has been found to be within 0.2–0.3, irrespective of the metal type, the nanoparticle size and shape, and the surrounding medium. This empirical scaling law has also been applied to Au nanorods that are linearly aligned.[19,21] However, due to the geometrical anisotropy of nanorods, the fitting of the data points for Au nanorods with eq 8 is not as good as that for Au and Ag nanoparticles.

We performed the FDTD calculations to determine the plasmon shift $\Delta\lambda/\lambda$ as a function of the gap distance d for homodimers of Au nanorods that have hemispherical ends and different aspect ratios (Figure 5). We first used eq 8 to fit the obtained data points, with the nanorod length treated as the characteristic size. However, for the aspect ratio from 1 to 4, the β and τ values
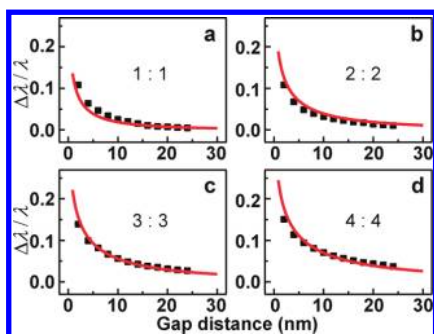
Figure 5. Gap-dependent fractional plasmon shifts in the homodimers of Au nanorods capped with hemispheres. The aspect ratios of the nanorods are (a) 1, (b) 2, (c) 3, and (d) 4. The coefficients of determination for the fittings are 0.9305, 0.9630, 0.9932, and 0.9859, respectively.

obtained from the fitting vary in the ranges 0.13−0.16 and 0.18−0.28, respectively. These results suggest that eq 8 is not good enough for predicting the coupled plasmon wavelengths of various Au nanorod homodimers. In order to have a more universal equation, we reasoned that the coupled plasmon energy is determined by the competition between the interparticle near-field interaction and the intraparticle Coulombic restoring force on the displaced electron cloud.[16] We therefore replaced the term d/D in eq 8 with $(V_{gap}/V_{nanorod})^{1/3}$, where V_{gap} and $V_{nanorod}$ denote the volumes of the gap region and nanorod, respectively. Because the volume ratio is approximately equal to d/L, with L being the nanorod length, the exponential equation can then be expressed as

$$\frac{\Delta\lambda}{\lambda} = \beta e^{-(d/L)^{1/3}/\tau} \qquad (9)$$

Figure 5 displays the calculated fractional plasmon shift as a function of the gap distance for different nanorod homodimers and the curves obtained from the fitting with eq 9. The coefficients of determination for all of the fittings are comparable to those for the fittings with eq 8. More importantly, all of the fittings give one set of β and τ at 0.67 and 0.22, respectively. The decay constant τ is very close to the values obtained previously for metal nanoparticles and nanorods.[11,14,15,19,21] With eq 9, we can calculate the coupled plasmon energies of Au nanorod homodimers and subsequently estimate the coupled plasmon energies of heterodimers composed of arbitrarily sized Au nanorods using the hyperbolic formula given in eq 3.

Figure 1b shows a blue-shifted weak scattering peak, in addition to the red-shifted strong peak, for the nanorod heterodimer. The weak scattering peak does not exhibit an anticrossing behavior in the plasmon coupling energy diagram. There is also a dip, which is located at the lower-energy side of the weak scattering peak. The weak scattering peak and the dip must arise from the symmetry breaking in the heterodimer because none of Au nanorod homodimers exhibit such

features. The appearance of the scattering peak agrees with previous experimental findings observed by us[22] and others.[39] The peaks on the calculated scattering spectra of the heterodimers have an asymmetric line shape, which signifies the Fano resonance.[29] The Fano resonance typically involves a broadband excitation light source, a superradiant mode, and a subradiant mode. The Fano profile is generated from the destructive interference between the two modes.[29]

In plasmonics, different coupled plasmon modes can be identified from corresponding spatial charge distributions. We therefore first calculated the charge distributions at different scattering energies for a heterodimer of Au nanorods with hemispherical ends in order to ascertain the coupled plasmon modes that are involved in the Fano resonance. The two nanorods have aspect ratios of 3.5 and 5. When they are placed together to form a heterodimer, the calculated scattering spectrum exhibits a weak peak at 1.610 eV (i), a dip at 1.533 eV (ii), and a strong peak at 1.254 eV (iii, Figure 6a). In comparison, the longitudinal plasmon energies of the two nanorod monomers are 1.587 and 1.297 eV, respectively (Figures 1a and 6b). The calculated charge distributions (Figure 6c) reveal that the strong scattering peak (iii) is contributed by the dipole−dipole bonding plasmon mode. At the positions of the weak scattering peak (i) and the dip (ii), the electron oscillation in the longer nanorod is mainly quadrupolar and slightly dipolar, and that in the shorter nanorod is dipolar. In order to obtain the hybridization energy diagram for the nanorod heterodimer, we also calculated the energies of the dipolar and quadrupolar plasmon modes of the longer nanorod by employing a dipole instead of a plane wave as the excitation source. The dipole source provides a nonuniform electromagnetic field. It can excite both the bright dipolar mode and the dark quadrupolar mode in the nanorod. Two peaks are seen on the obtained absorption spectrum of the longer nanorod (Figure 6b, red). The charge distributions (Figure 6c) at these two peaks show that the lower- (II) and higher-energy peaks (I) arise from the dipolar and quadrupolar plasmon mode, respectively. These two modes hybridize with the dipolar mode of the shorter nanorod to give the dipole−dipole and dipole−quadrupole bonding modes, as shown by the hybridization energy diagram in Figure 6a. The entire heterodimer therefore possesses a mixture of the hybridized dipole−dipole bonding and dipole−quadrupole bonding modes. The dipole−dipole bonding mode is superradiant. Its spectral profile extends to the energy region of the dipole−quadrupole bonding mode, as revealed by the charge distributions. The dipole−quadrupole bonding mode is subradiant. The destructive interference between the superradiant and subradiant modes gives rise to the asymmetric Fano profile of the scattering spectrum. The weak scattering peak in the nanorod heterodimers arises from the Fano resonance instead of
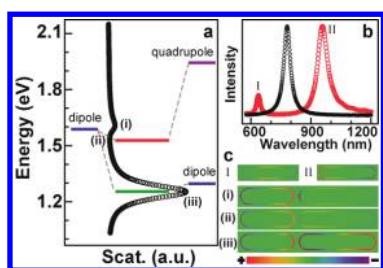
Figure 6. (a) Scattering spectrum and the plasmon hybridization diagram for a nanorod heterodimer. The nanorods have hemispherical ends. Their aspect ratios are 3.5 and 5. The gap distance is 7 nm. (i) and (iii) indicate the wavelengths of the two peaks, and (ii) indicates the valley between them. (b) Scattering spectrum of the shorter nanorod monomer (black circles) excited by a plane wave and the absorption spectrum of the longer nanorod monomer (red circles) excited by a dipole source. The absorption spectrum of the longer nanorod was calculated by replacing the shorter nanorod in the heterodimer with the dipole source at the center. In this way, both the quadrupolar (I) and dipolar (II) plasmon modes of the longer nanorod can be excited. (c) Charge distributions of the plasmon modes of the longer nanorod and hybridized plasmon modes in the heterodimer on the central cross sections of the nanorods.

the dipole–dipole antibonding mode. Therefore it does not exhibit an anticrossing behavior in the plasmon coupling energy diagram.

The asymmetric profiles of the calculated scattering spectra of the nanorod heterodimers can be well fitted by a phenomenological model in the form[51–54]

$$C_{sca}(\omega) = \left| a_r + \sum_{j=1,2} \frac{-b_j \Gamma_j e^{i\varphi_j}}{\hbar\omega - E_j + i\Gamma_j} \right|^2 \quad (10)$$

where C_{sca} represents the scattering signal, ω is the angular frequency, a_r denotes the background contribution, b_j, Γ_j, φ_j, and E_j represent the amplitude, line width, phase, and energy of each eigenmode, respectively, and $\hbar$ is Planck's constant divided by 2π. In our study, we consider only two plasmonic eigenmodes. One is the dipole–dipole bonding mode, which is denoted by the subscript 1, and the other is the dipole–quadrupole bonding mode, which is denoted by the subscript 2.

The Fano profile is strongly dependent on the plasmon energy difference and the gap distance between the two nanorod monomers in the heterodimer. Figure 7a shows the calculated scattering spectra of four representative nanorod heterodimers with the aspect ratio of one nanorod fixed at 5. Figure 7b shows the four representative spectra between the nanorods with aspect ratios of 3.5 and 5 at varying gap distances. In Figure 7a, as the aspect ratio of the varying nanorod becomes smaller and thus the dipolar plasmon energy of the nanorod becomes larger, both the dipole–dipole and dipole–quadrupole bonding modes shift to higher energies. At the same time, the intensity of the higher-energy scattering peak relative to that of the lower-energy one first grows larger and then gets
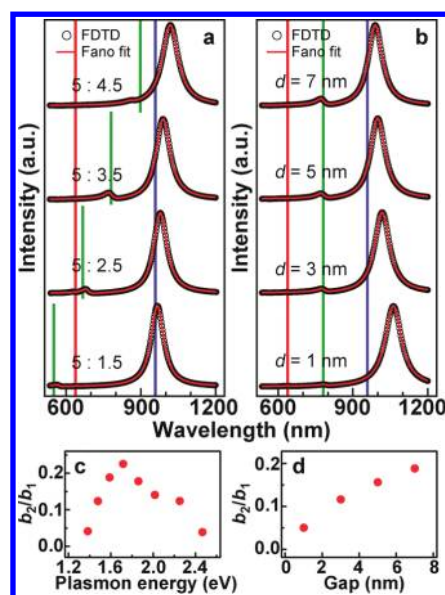

Figure 7. Fitting of the normalized scattering spectra of different Au nanorod heterodimers with the Fano profile. (a) The aspect ratio of one nanorod is fixed at 5, and that of the other nanorod is varied from 1 to 5. The gap between the two nanorods is 7 nm. (b) The aspect ratios of the two rods are fixed at 3.5 and 5. The gap is varied from 1 to 7 nm. The blue and red vertical bars indicate the dipolar and quadrupolar resonance positions of the longer nanorod, respectively, and the green ones indicate the dipolar resonance positions of the shorter nanorods. (c) Ratio of the amplitudes of the two eigenmodes obtained from the fitting versus the plasmon energy of the nanorod with varying aspect ratios. (d) Ratio of the amplitudes versus the gap distance between the two nanorods. The nanorods have hemispherical ends.

smaller. In Figure 7b, as the gap distance is gradually reduced, the higher-energy scattering peak gets weaker relative to the lower-energy one.

We fitted all of the calculated scattering spectra with the phenomenological model described in eq 10. The parameters obtained from the fitting are provided in Tables S10 and S11 in the Supporting Information. We found that the amplitude ratio, b_2/b_1, between the two plasmon eigenmodes can be utilized to describe the Fano interference strength between them. The closer the ratio is to 1, the more noticeable the asymmetric Fano profile will become and thereby the stronger the interference (Supporting Information, Figure S3). We therefore extracted b_2/b_1 and plotted them as a function of the plasmon energy of the varying nanorod in Figure 7c and as a function of the gap distance in Figure 7d. Figure 7c reveals that the 5: 3.5 nanorod heterodimer has the largest b_2/b_1 ratio and therefore the most distinct Fano resonance in the spectrum. The first increase and then decrease in the amplitude ratio is believed to result from the shift of the dipolar mode (1.297–2.466 eV, Supporting Information, Table S1) of the shorter nanorod from the red side to the blue side of the quadrupolar mode (1.944 eV, Figure 6b) of the longer nanorod. This shift causes the variation in the interference behavior between the two hybridized

modes. Moreover, for the 5:3.5 nanorod heterodimer, the Fano line shape becomes clearer as the gap distance is gradually increased (Figure 7d). The b_2/b_1 ratio is essentially determined by the relative strengths between the dipole−dipole and dipole−quadrupole bonding modes around their overlapping spectral region. The relative strengths of the two bonding modes are in turn affected by the gap distance and the aspect ratios of the nanorod monomers, the latter of which determine the energy levels before the hybridization. The variations of the b_2/b_1 ratios observed in our study reflect the interplay of the different factors on the Fano interference strength.

CONCLUSIONS

We have made a systematic investigation through FDTD calculations on the plasmon coupling energy diagrams of the dimers of Au nanorods that have varying aspect ratios and different capping ends. The nanorods are placed in a linear end-to-end manner. Their gap distance is also varied. All of the energy diagrams exhibit an anticrossing behavior. They can be rescaled into one universal curve and thereby described with a simple hyperbolic scaling formula. A model based on two coupled mechanical oscillators has been employed to assist in understanding the hyperbolic scaling law. Moreover, the symmetry breaking in Au nanorod heterodimers induces unambiguously a Fano profile in their scattering spectra. The calculated charge distributions reveal that the Fano resonance results from the interactions between the different plasmon eigenmodes in the nanorod heterodimers. The spectral position of the obtained Fano dip and the relative amplitudes between the interfering plasmon eigenmodes are found to be dependent on the aspect ratios of the nanorod monomers and the gap distance. From our point of view, the discovered hyperbolic scaling law will be applicable for the capacitive plasmon coupling between Au nanorods that have diameters of ∼5−50 nm and lengths of ∼10−200 nm. Such a range covers the sizes of typical colloidal Au nanorods that are prepared chemically. Quantum tunneling will take effect when the gap distance is less than ∼1 nm, and phase retardation will cause the excitation of multipolar plasmon modes and the hybridization of different plasmon modes for larger metal nanocrystals. Our results will be very useful in predicting the coupled plasmon energies of Au nanorod dimers for their applications in plasmon-enhanced spectroscopies, biological sensing, and nanoantennas. In addition, the variability of the Fano profiles in Au nanorod heterodimers offers an approach for the design of the Fano resonance, which can lead to new switchable metamaterials.

METHODS

During the FDTD calculations, an electromagnetic pulse in the wavelength range from 500 to 1200 nm was launched into a box containing the target nanostructure to simulate a propagating plane wave interacting with the nanostructure. The refractive index of the surrounding medium was taken to be 1.33 to simulate water. The dielectric function of gold was represented with a Drude model:

$$\varepsilon_D(\omega) = \varepsilon_\infty - \frac{\omega_D^2}{\omega^2 + i\gamma_D\omega} \tag{11}$$

The parameters in eq 11 are the high-frequency dielectric constant $\varepsilon_\infty = 9.5$, the plasma frequency $\omega_D = 13589.6$ THz, and the Drude damping constant $\gamma_D = 104.92$ THz.

Supporting Information Available: Plot of the linear dependence of the longitudinal plasmon wavelength on the aspect ratio of the Au nanorods, plasmon coupling energy diagrams calculated for the nanorod dimers immersed in different media, Fano profiles calculated for varying b_2/b_1 ratios, calculated plasmon energies of the Au nanorod monomers and dimers, and parameter values obtained from the fitting for the Fano profiles. This material is available free of charge *via* the Internet at http://pubs.acs.org.

REFERENCES AND NOTES

1. Sönnichsen, C.; Reinhard, B. M.; Liphardt, J.; Alivisatos, A. P. A Molecular Ruler Based on Plasmon Coupling of Single Gold and Silver Nanoparticles. *Nat. Biotechnol.* **2005**, *23*, 741–745.
2. Rosi, N. L.; Mirkin, C. A. Nanostructures in Biodiagnostics. *Chem. Rev.* **2005**, *105*, 1547–1562.
3. Large, N.; Abb, M.; Aizpurua, J.; Muskens, O. L. Photoconductively Loaded Plasmonic Nanoantennas as Building Block for Ultracompact Optical Switches. *Nano Lett.* **2010**, *10*, 1741–1746.
4. Kawata, S.; Ono, A.; Verma, P. Subwavelength Colour Imaging with a Metallic Nanolens. *Nat. Photonics* **2008**, *2*, 438–442.
5. Lim, D.-K.; Jeon, K.-S.; Kim, H. M.; Nam, J.-M.; Suh, Y. D. Nanogap-Engineerable Raman-Active Nanodumbbells for Single-Molecule Detection. *Nat. Mater.* **2010**, *9*, 60–67.
6. Kinkhabwala, A.; Yu, Z. F.; Fan, S. H.; Avlasevich, Y.; Müllen, K.; Moerner, W. E. Large Single-Molecule Fluorescence Enhancements Produced by a Bowtie Nanoantenna. *Nat. Photonics* **2009**, *3*, 654–657.
7. Schietinger, S.; Aichele, T.; Wang, H.-Q.; Nann, T.; Benson, O. Plasmon-Enhanced Upconversion in Single NaYF$_4$:Yb^{3+}/Er^{3+} Codoped Nanocrystals. *Nano Lett.* **2010**, *10*, 134–138.
8. Nevet, A.; Berkovitch, N.; Hayat, A.; Ginzburg, P.; Ginzach, S.; Sorias, O.; Orenstein, M. Plasmonic Nanoantennas for Broad-Band Enhancement of Two-Photon Emission from Semiconductors. *Nano Lett.* **2010**, *10*, 1848–1852.
9. Kim, S.; Jin, J.; Kim, Y.-J.; Park, I.-Y.; Kim, Y.; Kim, S.-W. High-Harmonic Generation by Resonant Plasmon Field Enhancement. *Nature* **2008**, *453*, 757–760.
10. Grigorenko, A. N.; Roberts, N. W.; Dickinson, M. R.; Zhang, Y. Nanometric Optical Tweezers Based on Nanostructured Substrates. *Nat. Photonics* **2008**, *2*, 365–370.
11. Su, K.-H.; Wei, Q.-H.; Zhang, X.; Mock, J. J.; Smith, D. R.; Schultz, S. Interparticle Coupling Effects on Plasmon Resonances of Nanogold Particles. *Nano Lett.* **2003**, *3*, 1087–1090.

12. Nordlander, P.; Oubre, C.; Prodan, E.; Li, K.; Stockman, M. I. Plasmon Hybridization in Nanoparticle Dimers. *Nano Lett.* **2004**, *4*, 899–903.

13. Atay, T.; Song, J.-H.; Nurmikko, A. V. Strongly Interacting Plasmon Nanoparticle Pairs: From Dipole–Dipole Interaction to Conductively Coupled Regime. *Nano Lett.* **2004**, *4*, 1627–1631.

14. Gunnarsson, L.; Rindzevicius, T.; Prikulis, J.; Kasemo, B.; Käll, M.; Zou, S. L.; Schatz, G. C. Confined Plasmons in Nanofabricated Single Silver Particle Pairs: Experimental Observations of Strong Interparticle Interactions. *J. Phys. Chem. B* **2005**, *109*, 1079–1087.

15. Jain, P. K.; Huang, W. Y.; El-Sayed, M. A. On the Universal Scaling Behavior of the Distance Decay of Plasmon Coupling in Metal Nanoparticle Pairs: A Plasmon Ruler Equation. *Nano Lett.* **2007**, *7*, 2080–2088.

16. Jain, P. K.; El-Sayed, M. A. Surface Plasmon Coupling and Its Universal Size Scaling in Metal Nanostructures of Complex Geometry: Elongated Particle Pairs and Nanosphere Trimers. *J. Phys. Chem. C* **2008**, *112*, 4954–4960.

17. Lassiter, J. B.; Aizpurua, J.; Hernandez, L. I.; Brandl, D. W.; Romero, I.; Lal, S.; Hafner, J. H.; Nordlander, P.; Halas, N. J. Close Encounters between Two Nanoshells. *Nano Lett.* **2008**, *8*, 1212–1218.

18. Willingham, B.; Brandl, D. W.; Nordlander, P. Plasmon Hybridization in Nanorod Dimers. *Appl. Phys. B: Laser Opt.* **2008**, *93*, 209–216.

19. Funston, A. M.; Novo, C.; Davis, T. J.; Mulvaney, P. Plasmon Coupling of Gold Nanorods at Short Distances and in Different Geometries. *Nano Lett.* **2009**, *9*, 1651–1658.

20. Aćimović, S. S.; Kreuzer, M. P.; González, M. U.; Quidant, R. Plasmon Near-Field Coupling in Metal Dimers as a Step toward Single-Molecule Sensing. *ACS Nano* **2009**, *3*, 1231–1237.

21. Tabor, C.; Van Haute, D.; El-Sayed, M. A. Effect of Orientation on Plasmonic Coupling between Gold Nanorods. *ACS Nano* **2009**, *3*, 3670–3678.

22. Shao, L.; Woo, K. C.; Chen, H. J.; Jin, Z.; Wang, J. F.; Lin, H.-Q. Angle- and Energy-Resolved Plasmon Coupling in Gold Nanorod Dimers. *ACS Nano* **2010**, *4*, 3053–3062.

23. Yang, S.-C.; Kobori, H.; He, C.-L.; Lin, M.-H.; Chen, H.-Y.; Li, C. C.; Kanehara, M.; Teranishi, T.; Gwo, S. Plasmon Hybridization in Individual Gold Nanocrystal Dimers: Direct Observation of Bright and Dark Modes. *Nano Lett.* **2010**, *10*, 632–637.

24. Huang, J.-S.; Kern, J.; Geisler, P.; Weinmann, P.; Kamp, M.; Forchel, A.; Biagioni, P.; Hecht, B. Mode Imaging and Selection in Strongly Coupled Nanoantennas. *Nano Lett.* **2010**, *10*, 2105–2110.

25. Sun, Z. H.; Ni, W. H.; Yang, Z.; Kou, X. S.; Li, L.; Wang, J. F. pH-Controlled Reversible Assembly and Disassembly of Gold Nanorods. *Small* **2008**, *4*, 1287–1292.

26. Merlein, J.; Kahl, M.; Zuschlag, A.; Sell, A.; Halm, A.; Boneberg, J.; Leiderer, P.; Leitenstorfer, A.; Bratschitsch, R. Nanomechanical Control of an Optical Antenna. *Nat. Photonics* **2008**, *2*, 230–233.

27. Huang, F. M.; Baumberg, J. J. Actively Tuned Plasmons on Elastomerically Driven Au Nanoparticle Dimers. *Nano Lett.* **2010**, *10*, 1787–1792.

28. Fan, J. A.; Wu, C.; Bao, K.; Bao, J. M.; Bardhan, R.; Halas, N. J.; Manoharan, V. N.; Nordlander, P.; Shvets, G.; Capasso, F. Self-Assembled Plasmonic Nanoparticle Clusters. *Science* **2010**, *328*, 1135–1138.

29. Luk'yanchuk, B.; Zheludev, N. I.; Maier, S. A.; Halas, N. J.; Nordlander, P.; Giessen, H.; Chong, C. T. The Fano Resonance in Plasmonic Nanostructures and Metamaterials. *Nat. Mater.* **2010**, *9*, 707–715.

30. Bachelier, G.; Russier-Antoine, I.; Benichou, E.; Jonin, C.; Del Fatti, N.; Vallée, F.; Brevet, P.-F. Fano Profiles Induced by Near-Field Coupling in Heterogeneous Dimers of Gold and Silver Nanoparticles. *Phys. Rev. Lett.* **2008**, *101*, 197401.

31. Sheikholeslami, S.; Jun, Y.-W.; Jain, P. K.; Alivisatos, A. P. Coupling of Optical Resonances in a Compositionally Asymmetric Plasmonic Nanoparticle Dimer. *Nano Lett.* **2010**, *10*, 2655–2660.

32. Brown, L. V.; Sobhani, H.; Lassiter, J. B.; Nordlander, P.; Halas, N. J. Heterodimers: Plasmonic Properties of Mismatched Nanoparticle Pairs. *ACS Nano* **2010**, *4*, 819–832.

33. Liu, N.; Weiss, T.; Mesch, M.; Langguth, L.; Eigenthaler, U.; Hirscher, M.; Sönnichsen, C.; Giessen, H. Planar Metamaterial Analogue of Electromagnetically Induced Transparency for Plasmonic Sensing. *Nano Lett.* **2010**, *10*, 1103–1107.

34. Liu, N.; Langguth, L.; Weiss, T.; Kästel, J.; Fleischhauer, M.; Pfau, T.; Giessen, H. Plasmonic Analogue of Electromagnetically Induced Transparency at the Drude Damping Limit. *Nat. Mater.* **2009**, *8*, 758–762.

35. Sámson, Z. L.; MacDonald, K. F.; De Angelis, F.; Gholipour, B.; Knight, K.; Huang, C. C.; Di Fabrizio, E.; Hewak, D. W.; Zheludev, N. I. Metamaterial Electro-Optic Switch of Nanoscale Thickness. *Appl. Phys. Lett.* **2010**, *96*, 143105.

36. Alù, A.; Engheta, N. Tuning the Scatting Response of Optical Nanoantennas with Nanocircuit Loads. *Nat. Photonics* **2008**, *2*, 307–310.

37. Mühlschlegel, P.; Eisler, H.-J.; Martin, O. J. F.; Hecht, B.; Pohl, D. W. Resonant Optical Antennas. *Science* **2005**, *308*, 1607–1609.

38. Prodan, E.; Radloff, C.; Halas, N. J.; Nordlander, P. A Hybridization Model for the Plasmon Response of Complex Nanostructures. *Science* **2003**, *302*, 419–422.

39. Slaughter, L. S.; Wu, Y. P.; Willingham, B. A.; Nordlander, P.; Link, S. Effects of Symmetry Breaking and Conductive Contact on the Plasmon Coupling in Gold Nanorod Dimers. *ACS Nano* **2010**, *4*, 4657–4666.

40. Nikoobakht, B.; El-Sayed, M. A. Preparation and Growth Mechanism of Gold Nanorods (NRs) Using Seed-Mediated Growth Method. *Chem. Mater.* **2003**, *15*, 1957–1962.

41. Sau, T. K.; Murphy, C. J. Seeded High Yield Synthesis of Short Au Nanorods in Aqueous Solution. *Langmuir* **2004**, *20*, 6414–6420.

42. Ni, W. H.; Kou, X. S.; Yang, Z.; Wang, J. F. Tailoring Longitudinal Surface Plasmon Wavelengths, Scattering and Absorption Cross Sections of Gold Nanorods. *ACS Nano* **2008**, *2*, 677–686.

43. Sudeep, P. K.; Joseph, S. T. S.; Thomas, K. G. Selective Detection of Cysteine and Glutathione Using Gold Nanorods. *J. Am. Chem. Soc.* **2005**, *127*, 6516–6517.

44. Zhang, S. Z.; Kou, X. S.; Yang, Z.; Shi, Q. H.; Stucky, G. D.; Sun, L. D.; Wang, J. F.; Yan, C. H. Nanonecklaces Assembled from Gold Rods, Spheres, and Bipyramids. *Chem. Commun.* **2007**, 1816–1818.

45. Chang, J.-Y.; Wu, H. M.; Chen, H.; Ling, Y.-C.; Tan, W. H. Oriented Assembly of Au Nanorods Using Biorecognition System. *Chem. Commun.* **2005**, 1092–1094.

46. Nie, Z. H.; Fava, D.; Kumacheva, E.; Zou, S.; Walker, G. C.; Rubinstein, M. Self-Assembly of Metal–Polymer Analogues of Amphiphilic Triblock Copolymers. *Nat. Mater.* **2007**, *6*, 609–614.

47. Nie, Z. H.; Fava, D.; Rubinstein, M.; Kumacheva, E. "Supramolecular" Assembly of Gold Nanorods End-Terminated with Polymer "Pom-Poms": Effect of Pom-Pom Structure on the Association Modes. *J. Am. Chem. Soc.* **2008**, *130*, 3683–3689.

48. Zhang, L.; Chen, H. J.; Wang, J. F.; Li, Y. F.; Wang, J.; Sang, Y.; Xiao, S. J.; Zhan, L.; Huang, C. Z. Tetrakis(4-sulfonatophenyl)porphyrin-Directed Assembly of Gold Nanocrystals: Tailoring the Plasmon Coupling through Controllable Gap Distances. *Small* **2010**, *6*, 2001–2009.

49. Garrido Alzar, C. L.; Martinez, M. A. G.; Nussenzveig, P. Classical Analog of Electromagnetically Induced Transparency. *Am. J. Phys.* **2002**, *70*, 37–41.

50. Mukherjee, S.; Sobhani, H.; Lassiter, J. B.; Bardhan, R.; Nordlander, P.; Halas, N. J. Fanoshells: Nanoparticles with Built-in Fano Resonances. *Nano Lett.* **2010**, *10*, 2694–2701.

51. Ropers, C.; Park, D. J.; Stibenz, G.; Steinmeyer, G.; Kim, J.; Kim, D. S.; Lienau, C. Femtosecond Light Transmission and Subradiant Damping in Plasmonic Crystals. *Phys. Rev. Lett.* **2005**, *94*, 113901.

52. Christ, A.; Ekinci, Y.; Solak, H. H.; Gippius, N. A.; Tikhodeev, S. G.; Martin, O. J. F. Controlling the Fano Interference in a Plasmonic Lattice. *Phys. Rev. B* **2007**, *76*, 201405.

53. Christ, A.; Martin, O. J. F.; Ekinci, Y.; Gippius, N. A.; Tikhodeev, S. G. Symmetry Breaking in a Plasmonic Metamaterial at Optical Wavelength. *Nano Lett.* **2008**, *8*, 2171–2175.

54. Verellen, N.; Van Dorpe, P.; Huang, C. J.; Lodewijks, K.; Vandenbosch, G. A. E.; Lagae, L.; Moshchalkov, V. V. Plasmon Line Shaping Using Nanocrosses for High Sensitivity Localized Surface Plasmon Resonance Sensing. *Nano Lett.* **2011**, *11*, 391–397.